



A lucky imaging multiplicity study of exoplanet host stars

C. Ginski,¹ M. Mugrauer, M. Seeliger and T. Eisenbeiss

Astrophysikalisches Institut und Universitäts-Sternwarte Jena, Jena 07743, Germany

Accepted 2012 January 2. Received 2012 January 2; in original form 2011 September 15

ABSTRACT

To understand the influence of additional wide stellar companions on planet formation, it is necessary to determine the fraction of multiple stellar systems amongst the known extrasolar planet population.

We target recently discovered radial velocity exoplanetary systems observable from the Northern hemisphere and with sufficiently high proper motion to detect stellar companions via direct imaging. We utilize the Calar Alto 2.2-m telescope in combination with its lucky imaging camera AstraLux.

71 planet host stars have been observed so far, yielding one new low-mass ($0.239 \pm 0.022 M_{\odot}$) stellar companion, 4.5 arcsec (227 au of projected separation) north-east of the planet host star HD 185269, detected via astrometry with AstraLux. We also present follow-up astrometry on three previously discovered stellar companions, showing for the first time common proper motion of the 0.5-arcsec companion to HD 126614. Additionally, we determined the achieved detection limits for all targets, which allow us to characterize the detection space of possible further companions of these stars.

Key words: techniques: high angular resolution – binaries: close – stars: individual: HD 126614 – stars: individual: HD 185269.

1 INTRODUCTION

Recent radial velocity (RV) and transiting exoplanet surveys have resulted in the discovery of a large number of new exoplanetary systems. Most stars are born in binary or multiple systems (Mathieu et al. 2000; Duchêne et al. 2007), and indeed we observe that a reasonable fraction of the stars in the Galaxy are multiple (Lada 2006). The effects of additional stellar companions on the planet formation process are therefore of high interest to constrain and calibrate planet formation theories.

A number of studies have been conducted on this subject in the past, such as described in Mugrauer, Seifahrt & Neuhauser (2007) or Daemgen et al. (2009) and most recently in Röll et al. (2011a) and Chauvin et al. (2011). As a result of these studies, 43 multiple stellar systems hosting exoplanets are known to date, suggesting that about 17 per cent of all known exoplanets reside in such systems (Mugrauer & Neuhauser 2009).

In this paper we present the results of our ongoing multiplicity study of the most recently (since 2008) discovered RV exoplanet host stars. We utilized the Calar Alto 2.2-m telescope and the AstraLux instrument (Hormuth et al. 2008) to achieve imaging data with higher Strehl ratio compared to simple seeing-limited imaging.

In the following section we characterize our sample. In Section 3 we give a brief introduction to the observation technique as well

as the instrument used and describe the reduction and astrometric calibration of our data. In Section 4 we show all confirmed or rejected companion candidates with the associated proper motion analysis. We also present detection limits for all studied systems. Finally in Section 5 we summarize our findings.

2 TARGET SAMPLE

Our sample consists of stars with RV planet candidates discovered between 2008 and 2011. They are all observable from the Northern hemisphere with declinations down to -22° and a relatively even distribution in right ascension. Since we want to test companionship of detected companion candidates via astrometry, we choose targets which are close enough to show a sufficient proper motion (e.g. >47 mas yr $^{-1}$ or approximately 1 AstraLux pixel yr $^{-1}$) to do a common proper motion analysis approximately one year after the first epoch images were taken. The distance distribution of our targets is shown in Fig. 1. On average our targets are 56.6 pc away and show a proper motion of 180.4 mas yr $^{-1}$ equivalent to 3.8 pixel yr $^{-1}$ on the AstraLux instrument.

The RV planet search technique favours main-sequence stars; therefore, the average age of our target stars is 4.6 Gyr (data as listed in exoplanet.eu by Schneider et al. 2011). Spectral types range from late F to early M, with the majority being G and K type. In Fig. 2 we show the metallicity distribution of our sample compared to the whole RV planet candidate host population. The average metallicity of our sample is slightly higher than solar metallicity at 0.09. The

*E-mail: ginski@astro.uni-jena.de

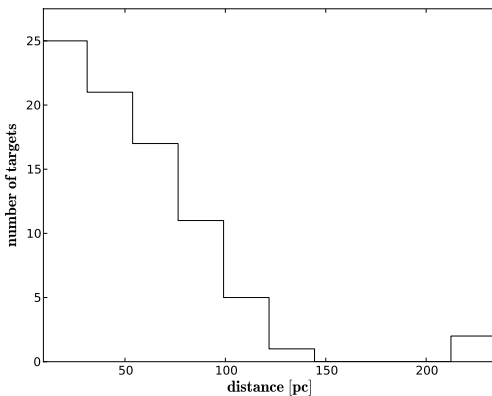


Figure 1. Histogram of distances of all our target stars (as listed in exoplanet.eu by Schneider et al. 2011). The majority is within 100 pc.

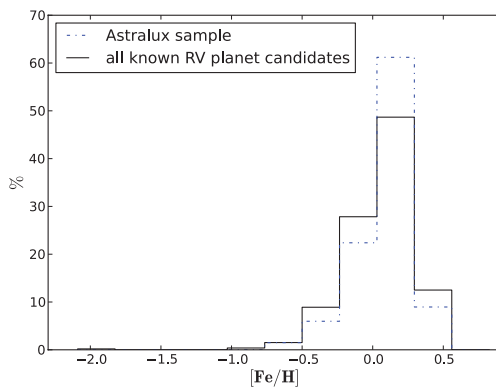


Figure 2. Metallicity distribution for all targets in our sample. For comparison we plot the metallicity distribution of all RV planet candidate host stars discovered so far (as listed in exoplanet.eu by Schneider et al. 2011).

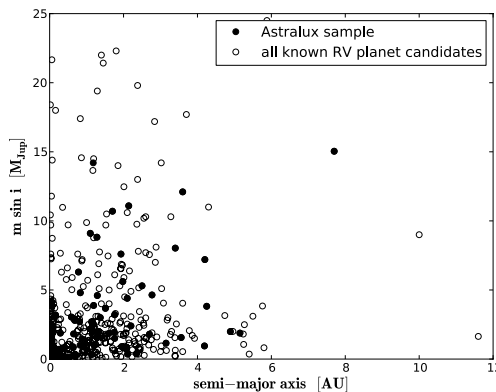


Figure 3. Minimum mass versus separation for all planet candidates orbiting hosts included in our sample (as listed in exoplanet.eu by Schneider et al. 2011). For comparison we also plot minimum mass versus separation of all RV planet candidates discovered so far.

metallicity distribution of our sample does not differ significantly from the whole population.

In Fig. 3 we present the minimum masses of detected RV planet candidates versus their semimajor axis for our sample and the whole population. The majority of the detected planet candidates are located within 2 au of their hosts. The average minimum mass of our sample is $2.8M_J$, as compared to $2.4M_J$ for the whole RV planet

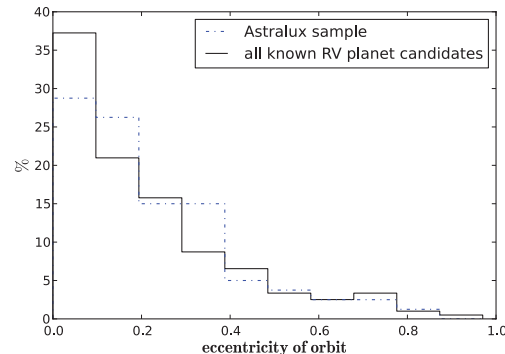


Figure 4. Eccentricity distribution of planet candidates orbiting hosts included in our sample. For comparison we also plot the eccentricity distribution of all RV planet candidates discovered so far (as listed in exoplanet.eu by Schneider et al. 2011).

candidate population. Given the standard deviation of $3.3M_J$ and $3.8M_J$, respectively, this is not significant.

The eccentricity distribution of RV planets around our sample stars can be seen in Fig. 4. We compared the eccentricity distribution of our sample to that of all RV planet candidates and found no significant differences.

We conclude that the general properties of our sample resemble those of the whole population.

3 OBSERVATION OUTLINE AND DATA CALIBRATION

3.1 Lucky imaging technique

To achieve high spatial resolution as well as high sensitivity, one must consider the effects of turbulent atmosphere. Given the Rayleigh criterion for the minimum resolvable angle of $\Theta = 1.22\lambda D^{-1}$, the Calar Alto 2.2-m telescope has a theoretical resolution of 89 mas at a wavelength of 776 nm, which is the central wavelength of the Sloan Digital Sky Survey (SDSS) i' filter that we are using. The median seeing at the Calar Alto site, however, is 0.9 arcsec (Sánchez et al. 2007), which is about 10 times larger.

The atmospheric conditions in the optical regime are subject to rapid variations with a time-scale that can be approximated by the speckle coherence time $\tau_e \approx 0.36r_0\Delta v^{-1}$ (Roddier, Gilli & Lund 1982), where r_0 is the Fried parameter and Δv is the wind speed dispersion in the atmosphere. For a typical wind speed dispersion of $\Delta v \approx 10 \text{ m s}^{-1}$ at the Calar Alto site and a V -band seeing of 0.7 arcsec, τ_e is of the order of 100 ms (Hormuth 2007). Within τ_e the resulting speckle pattern will remain fixed, whereas longer integration times would lead to an averaged and therefore ‘smeared out’ speckle pattern.

The lucky imaging approach consists of taking several thousand short images with integration times shorter than τ_e to sample the speckle variations during the observation window. We then only choose the so-called ‘lucky shots’ with a very high Strehl ratio in one of the speckles, to shift and add, resulting in a final image with the highest possible Strehl ratio and therefore the highest possible angular resolution.

For an in-depth introduction to the lucky imaging technique please see Law, Mackay & Baldwin (2006).

3.2 Observations and data reduction

All observations were carried out with the Calar Alto 2.2-m telescope in combination with the AstraLux instrument. This instrument consists of a back-illuminated, electron-multiplying, frame transfer CCD, which is well suited for the lucky imaging observation technique. For a detailed description of the instrument, see Hormuth et al. (2008).

Since we wanted to detect low-mass stellar or even brown dwarf companions of our targets, we chose the SDSS i' filter as described in Fukugita et al. (1996) for all observations. This is the best choice taking into account the sensitivity of the detector and the brightness of the detectable companions, as well as the variability of the atmosphere. For calibration we took dome- and sky-flats at the beginning and/or end of each observation night.

For all science targets we choose 29.54 ms of exposure time per frame, which is well below the typical speckle coherence time at the Calar Alto site. Shorter exposure times would have led to significantly growing overheads since we would have needed to switch off the frame transfer mode of the instrument. Longer exposure times would have resulted in a less localized and more ‘smeared out’ speckle pattern.

The electron-multiplying gain was individually adjusted for each target to obtain the maximum signal while still operating in the linear regime of the detector. We then took 100 dark frames with closed shutter and with the respective electron-multiplying settings before the start of each acquisition sequence.

Depending on weather conditions and time constraints we took between 10 000 and 80 000 frames per science target, which corresponds to a total integration time of 0.25 and 1.97 min, respectively, for a typical frame selection rate of 5 per cent. The obtained AstraLux images are all reduced and processed with our own European Southern Observatory Munich Image Data Analysis System (ESO-MIDAS) software for the reduction of imaging data taken with the lucky imaging technique. The individual AstraLux images are dark subtracted with the median (for optimal suppression of cosmic ray artefacts) of several short integrated dark frames and flat-fielded. For the lucky imaging data processing, the reached Strehl ratio in all individual images is determined at first using the bright planet host star as Strehl probe. The frames are then ranked according to their Strehl ratio and only the best 10, 5 and 1 per cent of all frames, i.e. only the frames with the highest Strehl ratio, are then selected and combined using the shift+add technique. Thereby, for image registration, the position of the brightest pixel in the speckle pattern of the planet host star is determined in all frames, which are then shifted and averaged.

3.3 Astrometric calibration

Since we want to precisely measure separation and position angle of our companion candidates with respect to the primary stars, and the AstraLux instrument is not permanently mounted to the Calar Alto 2.2-m telescope, a careful astrometric calibration of the detector in each observation epoch is necessary. For this purpose we selected a sample of five wide binaries, for which precise *Hipparcos* measurements as well as several additional observation epochs are available. We show our sample along with the *Hipparcos* astrometry in Table 1. Furthermore, we observed the centre of the globular cluster M15 whenever possible, for which precise *Hubble Space Telescope* (*HST*) astrometry is available.

For each epoch we have a minimum of three calibrators which were observed in the same night as the science targets. For all

Table 1. *Hipparcos* astrometry of epoch 1991.25 of our calibration binaries.

Binary	Separation (arcsec)	Position angle (°)
HIP 59585	18.677 ± 0.032	190.83 ± 0.10
HIP 65205	15.041 ± 0.015	219.44 ± 0.06
HIP 67099	18.751 ± 0.028	343.33 ± 0.09
HIP 72508	15.248 ± 0.014	91.36 ± 0.05
HIP 80953	16.356 ± 0.021	195.69 ± 0.07

Table 2. Astrometric calibration of all observation epochs. We list the pixel scale (PS) and the position angle (PA) of the y-axis for all observation epochs.

Epoch	PS (mas pixel $^{-1}$)	PA of y-axis (°)
23/04/2008	47.278 ± 0.101	0.17 ± 0.23
11/07/2008	47.180 ± 0.078	0.44 ± 0.15
16/01/2009	47.237 ± 0.114	359.39 ± 0.08
07/09/2009	47.220 ± 0.100	0.43 ± 0.13
23/02/2010	— ^a	— ^a
14/07/2010	47.243 ± 0.049	358.49 ± 0.22
14/01/2011	47.365 ± 0.135	358.07 ± 0.12
27/07/2011	47.160 ± 0.066	358.37 ± 0.23

^aDue to bad weather conditions no astrometric calibrators could be observed.

calibrators we used the *Hipparcos* measurement of epoch 1991.25 as reference point and then linearly fitted the slow orbital motion by using all data points available in the Washington Double Star (WDS) Catalog.

The pixel scales and position angles of the calibration images for each individual calibrator were calculated using ESO-MIDAS for the position measurements of the binary components, and Graphical Astronomy and Image Analysis Tool (GAIA) for the respective measurements of the M15 cluster components (using SExtractor: software for source extraction by Bertin & Arnouts 1996). The average of these calculations were used as final calibration for the respective epoch to cancel out systematic errors due to residual orbital motion of our binary stars. The final astrometric calibrations for all observation epochs are listed in Table 2.

3.4 PSF subtraction and astrometric measurements

Since we are searching for faint low-mass stellar companions to bright stars, we subtract the primary stars’ point spread function (PSF) in order to detect the companions with the highest possible signal-to-noise ratio. Due to the random nature of the lucky imaging approach, the PSFs in the final reduced images may vary significantly from star to star, for example, as a function of the average zenith distance of the observed objects. Hence it is not feasible to subtract a PSF standard from all the images. Furthermore, the PSFs of our target stars are not necessarily symmetrical in nature, rendering simple rotation subtraction techniques ineffective.

Given these limitations, we found the best approach to be an unsharp mask filter. We fold the images with a two-dimensional Gaussian of size n to ‘blur’ them, and then subtract the ‘blurred’ images from the originals, thus eliminating all low spatial frequencies from the images. We tested sizes n between 5 and 20 pixels for different images, with $n = 10$ generally yielding the best results in terms of improving the signal-to-noise ratio of the faint companion candidates.

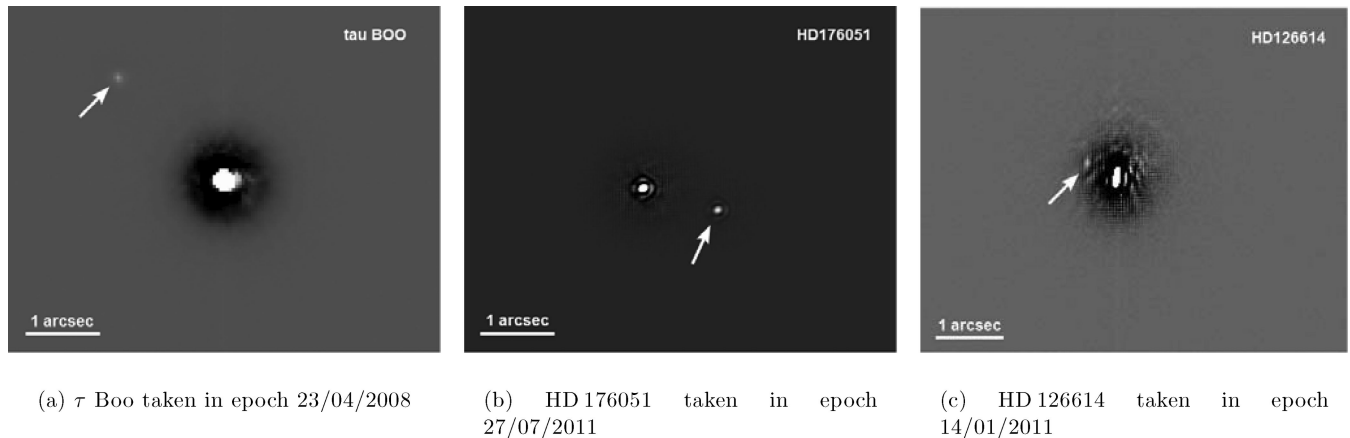


Figure 5. Follow-up images of already known companions to exoplanet host stars taken in SDSS i' filter during our ongoing campaign. All images have been PSF subtracted. North is always up and east to the left. The companions are marked by arrows.

We again used ESO-MIDAS for all astrometric measurements, first measuring the primary star's position in the original images, then applying the PSF subtraction as described, before measuring the companion candidate's position. We always measured both positions multiple times, averaging the results to avoid statistical errors.

4 RESULTS

To date we observed 71 planet host stars in our project. In seven cases we detected faint companion candidates, of which three were already known. In the following paragraphs, we show the astrometric measurements for all the companion candidates, as well as the proper motion analysis, to determine which of the objects are physically associated with the target stars.

4.1 Imaging of known companions

In the course of our study we imaged three already known companions to exoplanet hosts to test the instrument capabilities and to provide additional astrometric measurements for future orbit solutions. The final reduced images can be seen in Fig. 5 and our astrometric measurements are listed in Table 3.

The stellar companion to τ Boo resides at an angular separation of 2.181 ± 0.018 arcsec, which corresponds to a projected separation of 34 au. Patience et al. (2002) stated that τ Boo A and τ Boo B form an eccentric binary system with a semimajor axis of ≈ 225 au, and masses of ≈ 1.3 and $0.4 M_{\odot}$, respectively.

HD 176051 A and HD 176051 B form a close binary system of only 1.139 ± 0.009 arcsec separation and an orbital period of 61.2 yr. The stellar masses are 1.07 and $0.71 M_{\odot}$, respectively (Muterspaugh et al. 2010). Muterspaugh et al. (2010) found an

Table 3. Astrometric measurements of all known companions.

Primary	Epoch	Separation (arcsec)	Position angle ($^{\circ}$)
τ Boo	23/04/2008	2.181 ± 0.011	46.26 ± 0.42
HD 176051	27/07/2011	1.139 ± 0.005	252.12 ± 0.40
HD 126614	14/01/2011	0.499 ± 0.067	60.70 ± 5.60

astrometric companion of $\approx 1.5 M_{\odot}$, to be orbiting one of the components.

The stellar companion to HD 126614 was only detected recently by Howard et al. (2010) at the Palomar Observatory, using adaptive optics imaging. It is separated from the primary only by 0.490 ± 0.051 arcsec, which corresponds to a projected separation of 35.6 au. The mass of the companion was inferred from the JHK photometry to be $0.324 \pm 0.004 M_{\odot}$. Its companionship was so far only confirmed by photometry and RV trend. We are not aware of any further observations of this companion, especially regarding whether or not it is actually comoving with the primary. Hence we present a proper motion analysis in Section 4.3, using the measurements by Howard et al. (2010) and our own AstraLux data point, to confirm that HD 126614 A and HD 126614 B form indeed a common proper motion pair.

4.2 New companion candidates

In the course of our study we found new faint companion candidates around the planet host stars HD 185269, HD 183263, HD 187123 and HD 13931. In Fig. 6 we show the epochs with the highest signal-to-noise ratio.

In Table 4 we show all the astrometric measurements obtained in the different observation epochs for all companion candidates. Given the distances of the primary stars, the detected objects would have projected separations ranging from 179 au (close candidate of HD 187123) up to 781 au (far candidate of HD 187123).

4.3 Proper motion analysis

We performed a proper motion analysis for all companion candidates listed in Table 4 to distinguish between true physical companions and distant background objects. Hence we computed how separation and position angle would change from the first to the last observation epoch if the detected objects are indeed only in the background, and are therefore most likely standing still, also considering the effect of the annual parallax due to the Earth's motion around the Sun. We then compared these expected positions with the actual positions measured in our images. The resulting diagrams for all new companion candidates are listed in Fig. 7. Even if the detected objects are physically associated with the primaries, they might show a slightly different proper motion, which can be

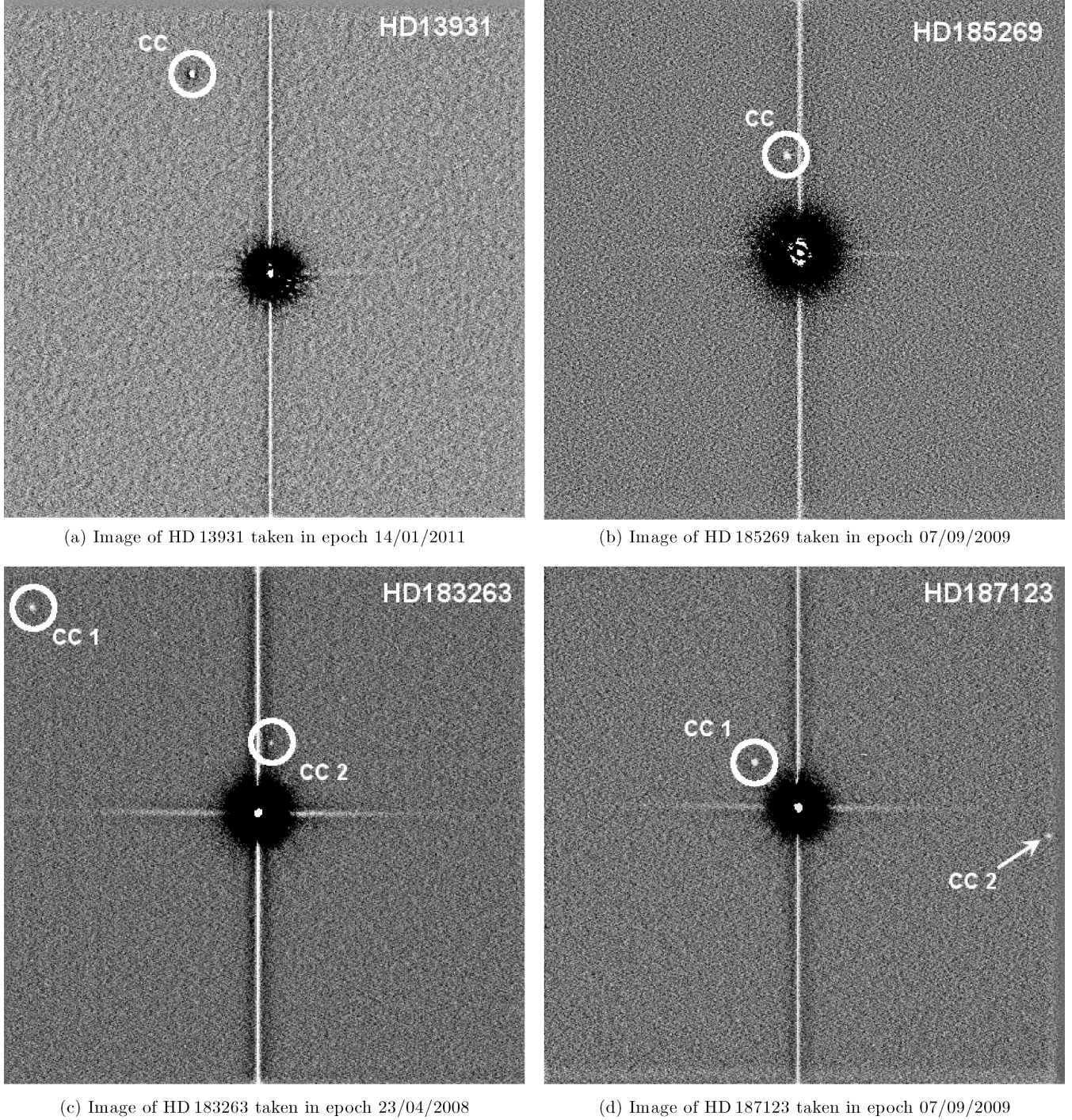


Figure 6. Images of our newly discovered companion candidates taken in SDSS i' filter. Images are 24.2×24.2 arcsec, north is always up and east to the left. In all cases the primary star's PSF was subtracted by an unsharp mask filter. Companion candidates are marked with circles and arrows. The numbers assigned to multiple companion candidates match those used in Table 4.

explained by orbital motion around the primary star. To account for this, we also added to the analysis the maximum possible change of separation and position angle due to orbital motion at the projected distance of our first epoch measurement. We assumed an edge-on circular orbit for changes in separation and a face-on circular orbit for changes in position angle, respectively.

HD 13931. HD 13931 was observed in 2011 January and July. The associated proper motion plot can be found in Fig. 7(a). The data

point taken in 2011 July is, within its uncertainty, consistent with the background and common proper motion hypotheses. The common proper motion hypothesis can be rejected only on the 0.83σ and 1.09σ level for separation and position angle, respectively; hence it is not possible to draw a final conclusion from our AstraLux measurements.

This companion candidate was resolved in Two Micron All Sky Survey (2MASS) J -, H - and K_s -band images taken on 1998

Table 4. Astrometric measurements of all companion candidates.

Primary	Epoch	No. of CC	Separation (arcsec)	Position angle ($^{\circ}$)
HD 13931	14/01/2011	1	9.972 ± 0.030	19.50 ± 0.16
	27/07/2011	1	10.003 ± 0.015	19.16 ± 0.25
HD 185269	07/09/2009	1	4.522 ± 0.014	7.91 ± 0.23
	14/07/2010	1	4.520 ± 0.010	8.17 ± 0.30
HD 183263	27/07/2011	1	4.511 ± 0.008	8.44 ± 0.28
	23/04/2008	1	14.190 ± 0.032	47.83 ± 0.26
HD 187123		2	3.295 ± 0.015	349.55 ± 0.40
	11/07/2008	1	14.183 ± 0.028	47.92 ± 0.19
		2	3.245 ± 0.017^a	349.72 ± 0.31^a
	07/09/2009	1	14.244 ± 0.033	47.93 ± 0.17
HD 187123		2	3.315 ± 0.031	350.75 ± 0.56
	11/07/2008	1	2.926 ± 0.011	48.11 ± 0.29
		2	11.560 ± 0.022	263.12 ± 0.19
	07/09/2009	1	2.917 ± 0.013	43.92 ± 0.29
		2	11.696 ± 0.028	263.92 ± 0.17

^aDue to the spurious detection of the companion candidate this data point seems dubious.

October 28. We show the corresponding K_s -band image in Fig. 8. Our measurements for this epoch yield a separation of 8.13 ± 0.15 arcsec and a position angle of 31.14 ± 0.75 . Using this new data point, we created a proper motion plot as shown in Fig. 9. Although the 2MASS data points are not consistent with the background hypothesis within 1σ , we can still reject common proper motion with 10.38σ for separation and 11.29σ for position angle. The inconsistency with the background hypothesis is most likely caused by a slow proper motion of the detected object. We conclude that our companion candidate around HD 13931 is only a background object.

HD 185269. In Fig. 7(b) we show the proper motion plot for the companion candidate next to HD 185269. Due to the overlap of the background and common proper motion areas in the position angle plot, our angular measurements would be consistent with both hypotheses. However, our measurements of the separation are only consistent with an object of common proper motion with the primary star. We can reject the background hypothesis with 9.9σ , and are therefore concluding that our object is indeed a previously unknown stellar companion to HD 185269. HD 185269 B has a projected separation of 227 au. Further follow-up observations will be executed to determine the orbital motion of the B component.

Using Image Reduction and Analysis Facility (IRAF) standard aperture photometry, we calculate an average magnitude difference of $\Delta I = 7.2 \pm 0.2$ mag throughout all our observation epochs. Given the age of the primary of 4.2 Gyr (Johnson et al. 2006) and the parallax of 21.11 ± 0.74 mas (van Leeuwen 2007), we find a mass of $0.239 \pm 0.022 M_{\odot}$, using the models by Baraffe et al. (1998).

HD 183263. Figs 7(c) and (d) show the proper motion plots for the two companion candidates discovered around HD 183263.

Due to the comparatively small proper motion of only 38.09 mas yr^{-1} (≈ 0.8 AstraLux pixel), a final conclusion for the first companion candidate is difficult with our epoch difference of 1.25 yr. The position angle gives no useful information, since the background and common proper motion areas are completely overlapping, and we can only reject the common proper motion hypothesis with 1.06σ , in the case of the separation. We could, however, identify our first companion candidate once more in the 2MASS catalogue. We show the corresponding image in K_s band in Fig. 10. The image was taken on 1999 August 5, giving us 10 yr

of epoch difference. The 2MASS Point Source Catalog (2MASS PSC; Cutri et al. 2003) measurements yield a separation of 13.8 ± 0.1 arcsec and a position angle of 48.2 ± 0.4 . Using this information, we created a new proper motion plot incorporating the 2MASS epoch which is shown in Fig. 11. Even though the error bars are significantly larger than the ones of our AstraLux measurements, the new proper motion analysis in separation clearly indicates that the first companion candidate around HD 183263 is a background object, with a significance of 3.3σ .

The second (closer) companion candidate was also detected in all three observation epochs. In 2008 July it was only barely visible, making these data points somewhat dubious. While the separation measurements are in general still consistent with a comoving object as well as a background object, the development of the position angle indicates (with 1.4σ corresponding to 83.8 per cent probability) that the second companion candidate is a background object as well.

HD 187123. The proper motion plots for the two companion candidates around HD 187123 are shown in Figs 7(e) and (f).

Both companion candidates show as fully consistent with the background hypothesis with an average significance level of 3.3σ . We conclude that both objects are indeed distant, non-moving background objects. HD 187123 is a single star within the given detection limits described in Section 4.4.

HD 126614. We also performed a proper motion analysis for the companion to HD 126614, using the measurements by Howard et al. (2010) as first epoch, and our own AstraLux measurement as second epoch. The resulting plot is shown in Fig. 12.

Our measured separation of 499 ± 67 mas and position angle of 60.7 ± 5.6 are consistent with the astrometry of the companion in the discovery epoch (489.0 ± 1.9 mas and 56.1 ± 0.3 , as given by Howard et al. 2010). However, due to the very low declination of $-05^{\circ} 10' 4''$, we had to observe HD 126614 at high air mass, which led to an extended PSF in the north–south direction. This made it very difficult to determine the position angle precisely, which is also evident in the large error bars of the measurement. Still the position angle is, within its error bars, consistent with common proper motion.

Despite the uncertainties in the position angle, we can still reject the background hypothesis with 1.7σ and 5.3σ for position

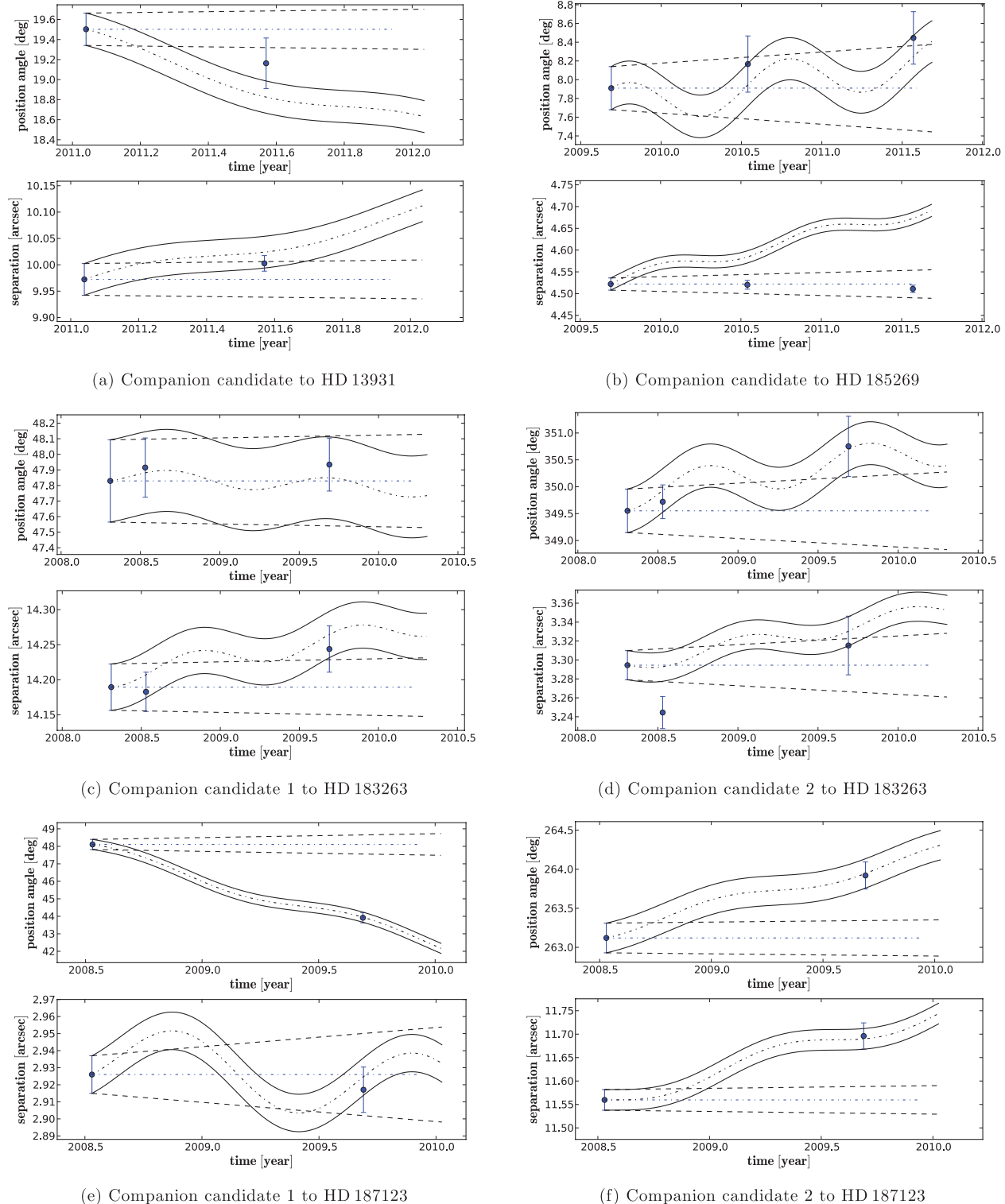


Figure 7. Proper motion diagrams for all newly discovered companion candidates. Upper diagrams are always for the position angle and lower diagrams for the separation, both plotted over time in years. The dashed lines mark the area for maximum possible orbital motion in the case of bound objects and circular orbits. The solid lines mark the area for non-moving background objects. The wobble in the background hypothesis is introduced by the annual parallax.

angle and separation, respectively. We can therefore conclude that HD 126614 B is indeed physically associated with A.

Due to the small separation between primary and companion, aperture photometry with *IRAF* is not viable. We could, however,

infer the *I*-band magnitude difference of companion and primary from the ratio of the peak counts. We calculate $\Delta I = 5.59 \pm 0.15$ mag. Given the $\log(\text{age}) = 9.1$ (Howard et al. 2010) and parallax of 14.63 ± 1.15 mas (van Leeuwen 2007), we find a mass of

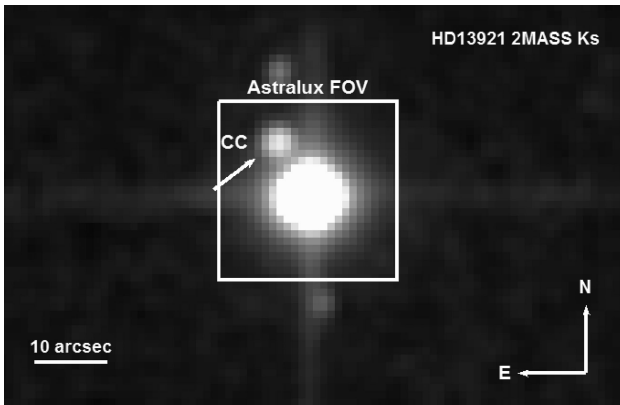


Figure 8. 2MASS K_s -band image of HD 13931 in epoch 1998 October 28. The Astralux field of view is indicated by the white rectangle.

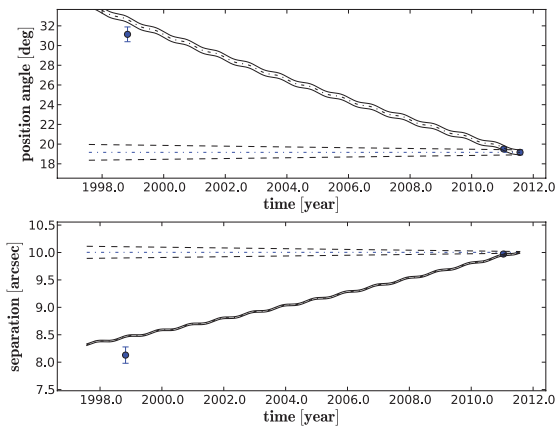


Figure 9. Proper motion diagram for the companion candidate to HD 13931 including a 2MASS measurement of epoch 1998 October 28. The areas for maximum orbital motion and background hypothesis are plotted backwards from our latest measurement in epoch 2011 July 27.

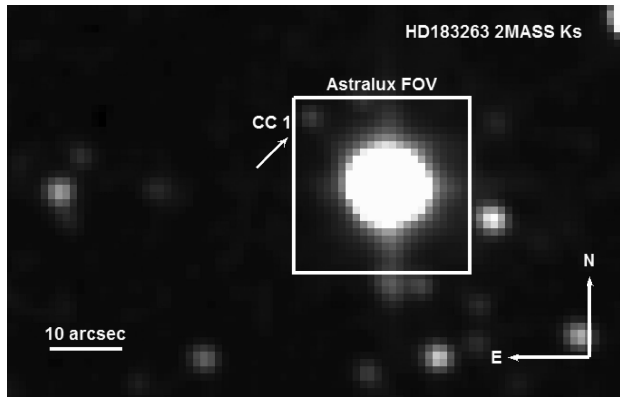


Figure 10. 2MASS K_s -band image of HD 183263 in epoch 1999 August 5. The Astralux field of view is indicated by the white rectangle.

$0.307 \pm 0.033 M_{\odot}$, using the models by Baraffe et al. (1998). This is consistent with the mass of 0.324 ± 0.004 found by Howard et al. (2010).

4.4 Detection limits and non-detections

In Fig. 13 we show the average dynamic range plots for each of our observation epochs. We determined the average dynamic range by

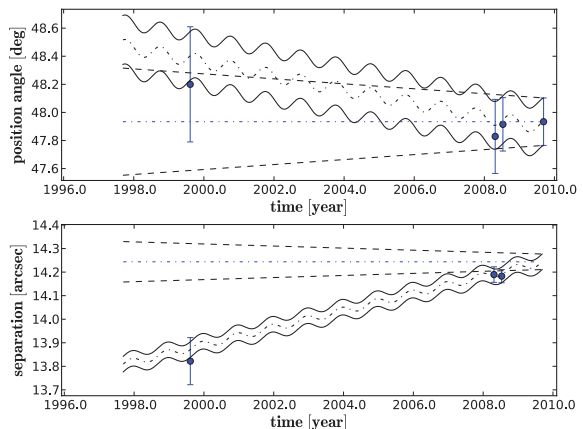


Figure 11. Proper motion diagram for the first (far) companion candidate to HD 183263 including a 2MASS measurement of epoch 1999 August. The areas for maximum orbital motion and background hypothesis are plotted backwards from our latest measurement in epoch 2009 September 7.

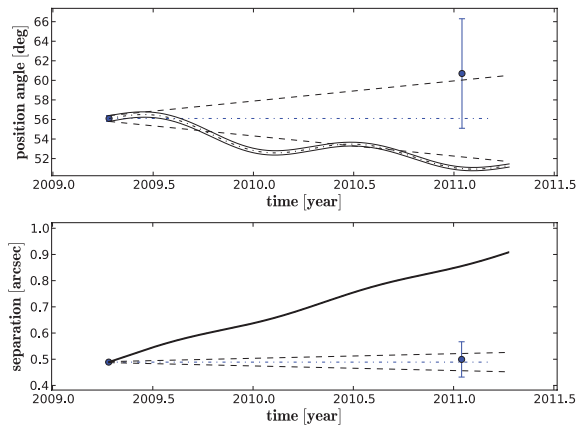


Figure 12. Proper motion diagrams for the stellar companion to HD 126614.

measuring the noise levels in all reduced images of a given epoch with a frame selection rate of 5 per cent, assuming a signal-to-noise ratio of 5. The primary stars' PSF was always subtracted to get the best possible results.

In all but two epochs we reach a magnitude difference of $\Delta I = 10$ mag outside of 2 arcsec from the primary star. Given the average absolute magnitudes and ages of the target stars in each epoch as listed in Table 5 (calculated from individual values as listed in Simbad and exoplanet.eu, respectively), and using the models by Baraffe et al. (1998), we would have easily been able to detect all wide stellar companions. Furthermore, we still probe the low-mass stellar regime ($M < 0.15 M_{\odot}$) down to separations of 1 arcsec from the primary star.

The observation epochs in 2009 January and 2010 February suffered from bad weather conditions, and while we could complete most of our observation programme in 2009 January, we could only observe for approximately one hour through the cloud cover in 2010 February. This is reflected in the dynamic range graphs in Figs 13(c) and (e), which show a noticeable decline in sensitivity in comparison with the other observation epochs. On average we are still able to detect stellar companions down to $0.15 M_{\odot}$ outside of 1.2 and 3.1 arcsec, respectively.

In Tables 6 and 7 we list all the systems that were observed in our survey to date, with and without additional stellar components detected, respectively. We also list the epochs in which these systems

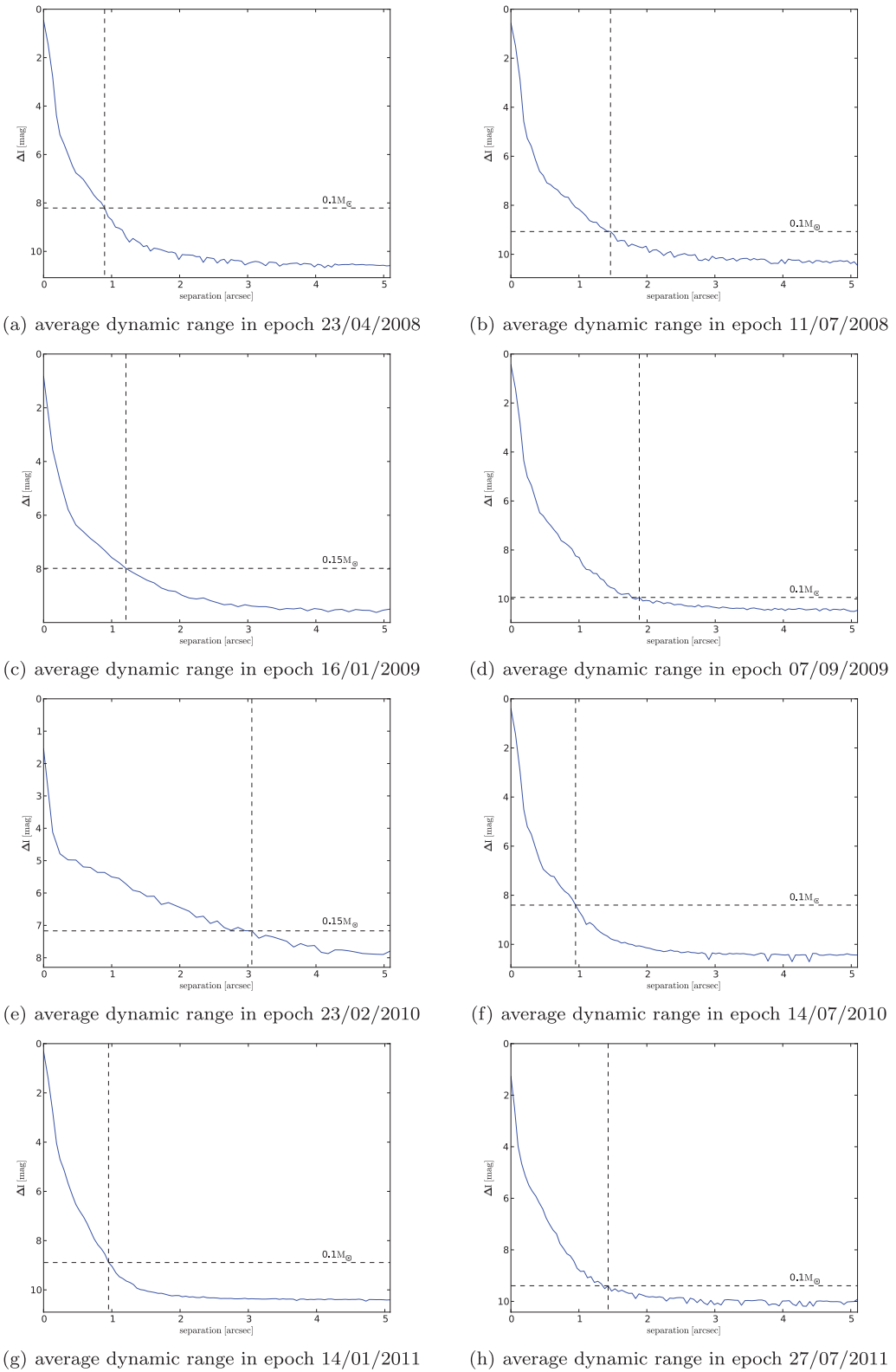


Figure 13. Average dynamic range plots for a signal-to-noise ratio of 5 for all our observation epochs. The dashed lines represent the detectable minimum mass objects at a given separation from the primary star, using the model by Baraffe et al. (1998). The primary stars' PSF was always subtracted by unsharp mask filtering before determining the dynamic range.

Table 5. Average absolute magnitudes and ages of all target stars in an observation epoch.

Epoch	MI (mag)	Age (Gyr)
23/04/2008	4.32	4.9
11/07/2008	3.43	6.0
16/01/2009	2.93	4.6
07/09/2009	2.64	6.2
23/02/2010	3.72	2.2
14/07/2010	4.14	7.4
14/01/2011	3.67	5.4
27/07/2011	3.20	6.5

have been observed, since our detection limits vary with the weather and seeing conditions. Additionally we present limits for the lowest mass objects detectable at separations of 0.5, 1, 2 and 5 arcsec, at a signal-to-noise ratio of 5, in the PSF-subtracted images. We calculated the uncertainties of these mass limits considering the uncertainties in the measured parallaxes for each system, as well as a maximum photometric error of 0.2 mag in our AstraLux images, along with an average photometric error of 0.05 mag in the primary stars' *I*-band magnitudes.

If we average all minimum masses for the respective separations as derived in Table 7, we conservatively get detection limits of $0.34 M_{\odot}$ at 0.5 arcsec as well as $0.22 M_{\odot}$ at 1 arcsec and $0.15 M_{\odot}$ outside of 2 arcsec. Given our field of view, we can detect such low-mass stellar companions up to separations of 12 arcsec.

5 CONCLUSIONS

In our ongoing study we observed 71 planet host stars to date. Of these 71 systems, three were already known to be multiple, for which we present follow-up astrometry. Thereby, we show for the first time conclusively that the companion to HD 126614 is indeed physically associated with the primary. As the planet host star HD 126614 also exhibits a further companion at a wider separation [HD 216614 C, sep = 41.914 ± 0.110 arcsec (3043 au), PA = $299:36 \pm 0:14$ at 2MASS epoch 2000 May 3], the HD 126614 system is actually a hierarchical triple system, the only one presently known in which the planet host star exhibits a close stellar companion. All other

known planet host triples are composed of the planet host star and a binary companion at wider separation.

We also discovered one new low-mass ($0.239 \pm 0.022 M_{\odot}$) stellar companion to the star HD 185269, with a separation of 4.511 ± 0.013 arcsec at a position angle of $8:44 \pm 0:30$. This corresponds to a projected distance of 227 au. HD 185269A harbours a 'hot Jupiter' ($M \sin i = 0.94 M_{\oplus}$) with an orbital period of 6.8 d and a semimajor axis of 0.077 au, detected by Johnson et al. (2006). They state that its orbital eccentricity of 0.3 is large in comparison with other planets found within 1 au of their host stars. This could possibly be explained by the Kozai mechanism as described by Takeda & Rasio (2005). We used the formula

$$P \simeq 2\pi \sqrt{\frac{a_1^3}{G(m_0 + m_1)}} \left(\frac{m_0 + m_1}{m_2} \right) \left(\frac{a_2}{a_1} \right)^3 (1 - e_2^2)^{3/2}$$

to calculate the period of the Kozai oscillations (Ford, Kozinsky & Rasio 2000), where the indices 0, 1 and 2 represent the host star, planetary and stellar companions, respectively. Assuming an eccentricity of 0.5 for the stellar companion (as suggested by statistical analysis in Söderhjelm 1999), and a semimajor axis equal to the projected separation of 227 au, we get a period of 1.7 Gyr. Given the age of HD 185269 A of 4.2 Gyr, this period is short enough so that the Kozai effect might have altered the planetary companion's eccentricity and inclination.

For the remaining 66 target stars in our sample we can on average exclude all low-mass stellar companions of $M > 0.15 M_{\odot}$ down to 2 arcsec around the primary. For many stars in our sample we get significantly deeper, enabling us to exclude all low-mass stellar companions outside of 2 arcsec and up to 12 arcsec. To further summarize our detection limits, in Fig. 14 we show the average dynamic range plot of all observations, with all detected stellar companions marked.

68 stars of our sample had an unknown multiplicity status before our observations. Of those, only one proved to be multiple within the detection limits of our survey. This yields a multiplicity rate of only 1.5 per cent for our sample. Given that the multiplicity rate of the known exoplanet host population is about 17 per cent, stellar multiple systems are underrepresented in our sample. However, since the sample size of our AstraLux survey is not yet statistically significant (≥ 231 for 95 per cent confidence level and an error margin of 5 per cent) we cannot draw any conclusion for the whole exoplanet population. For a detailed statistical analysis of the properties of all

Table 6. List of all stars with companions and companion candidates detected. We give the numbers of frames observed, each frame with an exposure time of 29.54 ms. We also give an upper limit for the minimum mass detectable at 0.5, 1, 2 and 5 arcsec using the models by Baraffe et al. (1998) and assuming an average age for each epoch as listed in Table 5.

Star	Epoch	No. of frames	$M (M_{\odot})$ at 0.5 arcsec	$M (M_{\odot})$ at 1 arcsec	$M (M_{\odot})$ at 2 arcsec	$M (M_{\odot})$ at 5 arcsec
HD13931	14/01/2011	50 000	0.173 ± 0.014	0.097 ± 0.003	0.086 ± 0.001	0.085 ± 0.001
	27/07/2011	50 000	0.365 ± 0.036	0.142 ± 0.010	0.105 ± 0.004	0.100 ± 0.004
HD183263	23/04/2008	50 000	0.194 ± 0.020	0.099 ± 0.003	0.086 ± 0.001	0.085 ± 0.001
	11/07/2008	80 000	0.180 ± 0.016	0.144 ± 0.011	0.099 ± 0.003	0.088 ± 0.002
	07/09/2009	80 000	0.178 ± 0.015	0.096 ± 0.003	0.087 ± 0.001	0.086 ± 0.002
HD187123	11/07/2008	77 800	0.149 ± 0.010	0.103 ± 0.004	0.086 ± 0.001	0.083 ± 0.001
	07/09/2009	80 000	0.160 ± 0.012	0.091 ± 0.002	0.084 ± 0.001	0.084 ± 0.001
HD185269	07/09/2009	50 000	0.307 ± 0.032	0.166 ± 0.013	0.107 ± 0.005	0.096 ± 0.003
	14/07/2010	60 000	0.286 ± 0.027	0.125 ± 0.007	0.093 ± 0.003	0.091 ± 0.002
	27/07/2011	50 000	0.239 ± 0.021	0.113 ± 0.006	0.091 ± 0.002	0.089 ± 0.002
τ Boo	23/04/2008	50 000	0.208 ± 0.019	0.104 ± 0.004	0.088 ± 0.001	0.088 ± 0.001
HD176051	27/07/2011	50 000	0.149 ± 0.010	0.095 ± 0.003	0.084 ± 0.001	0.084 ± 0.001
HD126614	14/01/2011	50 000	0.179 ± 0.018	0.103 ± 0.005	0.090 ± 0.002	0.088 ± 0.002

Table 7. List of all stars with no additional stellar components detected. We give the numbers of frames observed, each frame with an exposure time of 29.54 ms. We also give an upper limit for the minimum mass detectable at 0.5, 1, 2 and 5 arcsec using the models by Baraffe et al. (1998) and assuming an average age for each epoch as listed in Table 5.

Star	RA	Dec.	Epoch	No. of frames	$M (M_{\odot})$ at 0.5 arcsec	$M (M_{\odot})$ at 1 arcsec	$M (M_{\odot})$ at 2 arcsec	$M (M_{\odot})$ at 5 arcsec
HD 1461	00 18 41.8	-08 03 10.8	14/07/2010	55 000	0.157 ± 0.011	0.099 ± 0.003	0.083 ± 0.001	0.082 ± 0.001
BD-1763	00 28 34.3	-16 13 34.8	07/09/2009	50 000	0.110 ± 0.006	0.091 ± 0.003	0.083 ± 0.001	0.079 ± 0.001
Hat-P-19	00 38 04.0	+34 42 41.6	27/07/2011	50 000	0.140 ± 0.022	0.109 ± 0.012	0.099 ± 0.008	0.098 ± 0.007
HD 4203	00 44 41.2	+20 26 56.1	11/07/2008	80 000	0.176 ± 0.020	0.117 ± 0.008	0.091 ± 0.003	0.086 ± 0.002
HD 5319	00 55 01.4	+00 47 22.4	11/07/2008	50 000	0.424 ± 0.047	0.221 ± 0.027	0.140 ± 0.013	0.128 ± 0.011
HIP 5158	01 06 02.0	-22 27 11.3	14/01/2011	50 000	0.112 ± 0.008	0.089 ± 0.002	0.080 ± 0.002	0.079 ± 0.001
HD 6718	01 07 48.6	-08 14 01.3	14/01/2011	50 000	0.211 ± 0.021	0.107 ± 0.005	0.085 ± 0.001	0.083 ± 0.001
HD 7924	01 21 59.1	+76 42 37.0	27/07/2011	50 000	0.100 ± 0.003	0.082 ± 0.001	0.079 ± 0.001	0.078 ± 0.001
HD 8673	01 26 08.7	+34 34 46.9	14/01/2011	50 000	0.270 ± 0.025	0.113 ± 0.006	0.089 ± 0.002	0.088 ± 0.001
HD 9446	01 33 20.1	+29 15 54.5	14/07/2010	55 000	0.148 ± 0.011	0.099 ± 0.003	0.086 ± 0.001	0.083 ± 0.002
HD 16232	02 37 00.5	+24 38 49.9	23/02/2010	20 000	0.402 ± 0.033	0.318 ± 0.034	0.208 ± 0.022	0.121 ± 0.007
HD 16175	02 37 01.9	+42 03 45.4	27/07/2011	50 000	0.236 ± 0.024	0.108 ± 0.005	0.093 ± 0.003	0.091 ± 0.003
HD 16760	02 42 21.3	+38 37 07.2	23/02/2010	20 000	0.289 ± 0.047	0.223 ± 0.036	0.159 ± 0.019	0.108 ± 0.009
HD 17092	02 46 22.1	+49 39 11.1	14/07/2010	55 000	0.441 ± 0.181	0.213 ± 0.122	0.121 ± 0.043	0.112 ± 0.035
HIP 12961	02 46 42.8	-23 05 11.8	14/01/2011	50 000	0.105 ± 0.004	0.077 ± 0.001	0.074 ± 0.001	0.074 ± 0.001
HD 17156	02 49 44.4	+71 45 11.6	23/02/2010	20 000	0.465 ± 0.038	0.376 ± 0.038	0.243 ± 0.027	0.136 ± 0.010
HD 22781	03 40 49.5	+31 49 34.6	27/07/2011	50 000	0.112 ± 0.005	0.086 ± 0.001	0.079 ± 0.001	0.078 ± 0.001
HD 28305 ^a	04 28 36.9	+19 10 49.5	07/09/2009	10 000	0.862 ± 0.031	0.653 ± 0.028	0.342 ± 0.036	0.325 ± 0.034
HD 32518	05 09 36.7	+69 38 21.8	14/01/2011	50 000	0.686 ± 0.036	0.259 ± 0.030	0.183 ± 0.020	0.185 ± 0.020
HD 34445	05 17 40.9	+07 21 12.0	14/01/2011	50 000	0.219 ± 0.020	0.094 ± 0.003	0.089 ± 0.002	0.089 ± 0.002
HD 33564	05 22 33.5	+79 13 52.1	07/09/2009	50 000	0.253 ± 0.022	0.148 ± 0.009	0.097 ± 0.003	0.095 ± 0.002
HD 38801	05 47 59.1	-08 19 39.7	14/01/2011	50 000	0.363 ± 0.065	0.115 ± 0.012	0.097 ± 0.006	0.095 ± 0.005
HD 45652	06 29 13.2	+10 56 02.0	16/01/2009	22 610	0.165 ± 0.013	0.118 ± 0.007	0.094 ± 0.003	0.087 ± 0.001
HD 45410	06 30 47.1	+58 09 45.4	14/01/2011	50 000	0.474 ± 0.034	0.198 ± 0.019	0.127 ± 0.008	0.124 ± 0.007
HD 68988	08 18 22.1	+61 27 38.5	23/04/2008	50 000	0.177 ± 0.015	0.120 ± 0.007	0.092 ± 0.003	0.084 ± 0.002
HD 73534	08 39 15.8	+12 57 37.3	14/01/2011	50 000	0.287 ± 0.041	0.107 ± 0.007	0.093 ± 0.004	0.093 ± 0.003
HD 74156	08 42 25.1	+04 34 41.1	16/01/2009	16 000	0.386 ± 0.040	0.216 ± 0.023	0.141 ± 0.011	0.131 ± 0.009
HD 75898	08 53 50.8	+33 03 24.5	23/04/2008	50 000	0.222 ± 0.027	0.130 ± 0.010	0.096 ± 0.003	0.091 ± 0.003
HD 81688	09 28 39.9	+45 36 05.3	14/01/2011	48 149	0.647 ± 0.032	0.291 ± 0.034	0.216 ± 0.024	0.216 ± 0.024
HD 87883	10 08 43.1	+34 14 32.1	14/01/2011	50 000	0.107 ± 0.004	0.084 ± 0.001	0.078 ± 0.001	0.078 ± 0.001
HD 90043	10 23 28.3	-00 54 08.0	14/01/2011	50 000	0.553 ± 0.032	0.183 ± 0.017	0.125 ± 0.008	0.126 ± 0.008
HIP 57050	11 41 44.6	+42 45 07.1	14/01/2011	50 000	< 0.072	< 0.072	< 0.072	< 0.072
GJ 436	11 42 11.1	+26 42 23.7	11/07/2008	80 000	0.080 ± 0.001	0.076 ± 0.001	0.073 ± 0.001	< 0.072
HD 104985	12 05 15.1	+76 54 20.6	16/01/2009	26 480	0.682 ± 0.030	0.518 ± 0.034	0.253 ± 0.025	0.238 ± 0.023
HD 107148	12 19 13.5	-03 19 11.2	16/01/2009	50 000	0.214 ± 0.021	0.147 ± 0.011	0.102 ± 0.004	0.090 ± 0.002
HD 109246	12 32 07.1	+74 29 22.3	14/01/2011	50 000	0.157 ± 0.012	0.098 ± 0.003	0.087 ± 0.001	0.083 ± 0.001
HD 110014	12 39 14.7	-07 59 44.0	14/01/2011	50 000	0.881 ± 0.041	0.534 ± 0.037	0.298 ± 0.037	0.287 ± 0.035
HD 114783	13 12 43.7	-02 15 54.1	23/04/2008	50 000	0.125 ± 0.006	0.086 ± 0.001	0.078 ± 0.001	0.077 ± 0.001
HD 115617	13 18 24.3	-18 18 40.3	14/01/2011	50 000	0.611 ± 0.025	0.354 ± 0.031	0.158 ± 0.011	0.155 ± 0.011
HD 118203	13 34 02.5	+53 43 42.7	23/04/2008	50 000	0.249 ± 0.028	0.123 ± 0.008	0.096 ± 0.003	0.092 ± 0.003
HD 125612 A	14 20 53.5	-17 28 53.4	23/04/2008	50 000	0.194 ± 0.021	0.130 ± 0.009	0.098 ± 0.003	0.087 ± 0.002
HD 128311	14 36 00.6	+09 44 47.4	14/01/2011	50 000	0.106 ± 0.004	0.083 ± 0.001	0.077 ± 0.001	0.077 ± 0.001
HD 132406	14 56 54.7	+53 22 55.8	16/01/2009	32 000	0.200 ± 0.021	0.139 ± 0.010	0.106 ± 0.005	0.093 ± 0.003
HD 136418	15 19 06.1	+41 43 59.5	27/07/2011	50 000	0.463 ± 0.041	0.178 ± 0.017	0.109 ± 0.006	0.099 ± 0.004
HD 137759	15 24 55.7	+58 57 57.8	11/07/2008	60 000	0.709 ± 0.026	0.467 ± 0.030	0.202 ± 0.017	0.191 ± 0.017
HD 142091	15 51 13.9	+35 39 26.6	16/01/2009	16 000	0.549 ± 0.027	0.422 ± 0.033	0.233 ± 0.019	0.157 ± 0.011
HD 145675	16 10 24.3	+43 49 03.5	11/07/2008	80 000	0.130 ± 0.007	0.098 ± 0.002	0.083 ± 0.001	0.081 ± 0.001
HD 148427	16 28 28.1	-13 23 58.6	14/07/2010	55 000	0.371 ± 0.038	0.163 ± 0.013	0.098 ± 0.003	0.093 ± 0.003
HD 149026	16 30 29.6	+38 20 50.3	07/09/2009	50 000	0.242 ± 0.025	0.128 ± 0.008	0.097 ± 0.003	0.092 ± 0.003
HD 150706	16 31 17.5	+79 47 23.2	07/09/2009	50 000	0.160 ± 0.011	0.103 ± 0.004	0.086 ± 0.001	0.083 ± 0.001
HD 149143	16 32 51.0	+02 05 05.3	23/04/2008	50 000	0.225 ± 0.023	0.103 ± 0.005	0.088 ± 0.002	0.087 ± 0.002
GL 649	16 58 08.8	+25 44 38.9	14/07/2010	40 950	0.080 ± 0.001	0.074 ± 0.001	< 0.072	< 0.072
HD 154345	17 02 36.4	+47 04 54.7	07/09/2009	50 000	0.139 ± 0.009	0.098 ± 0.003	0.083 ± 0.001	0.079 ± 0.001
HD 155358	17 09 34.6	+33 21 21.0	14/07/2010	53 240	0.174 ± 0.013	0.101 ± 0.003	0.086 ± 0.001	0.085 ± 0.001
GJ 1214	17 15 18.9	+04 57 49.7	14/07/2010	55 000	0.075 ± 0.001	< 0.072	< 0.072	< 0.072
HD 156668	17 17 40.4	+29 13 38.0	14/07/2010	55 000	0.101 ± 0.003	0.086 ± 0.001	0.078 ± 0.001	0.077 ± 0.001
HD 164922	18 02 30.8	+26 18 46.8	07/09/2009	50 000	0.133 ± 0.008	0.096 ± 0.003	0.082 ± 0.001	0.080 ± 0.001
HD 167042	18 10 31.6	+54 17 11.5	07/09/2009	50 000	0.484 ± 0.028	0.256 ± 0.022	0.130 ± 0.008	0.108 ± 0.005
HD 170693	18 25 59.1	+65 33 48.5	14/07/2010	55 000	0.764 ± 0.028	0.542 ± 0.029	0.279 ± 0.028	0.286 ± 0.031
HD 173416	18 43 36.1	+36 33 23.7	27/07/2011	50 000	0.741 ± 0.033	0.419 ± 0.040	0.247 ± 0.027	0.242 ± 0.026
HD 188310	19 54 14.8	+08 27 41.2	07/09/2009	50 000	0.667 ± 0.030	0.455 ± 0.039	0.187 ± 0.019	0.161 ± 0.014
HD 200964	21 06 39.8	+03 48 11.2	27/07/2011	50 000	0.356 ± 0.040	0.144 ± 0.012	0.116 ± 0.007	0.112 ± 0.006
HD 218566	23 09 10.7	-02 15 38.6	27/07/2011	50 000	0.107 ± 0.004	0.084 ± 0.001	0.079 ± 0.001	0.078 ± 0.001
HD 221345	23 31 17.4	+39 14 10.3	07/09/2009	50 000	0.653 ± 0.028	0.365 ± 0.036	0.183 ± 0.017	0.169 ± 0.014

^aThe companion candidate (Mason et al. 2009) at 0.237 arcsec separation could not be resolved.

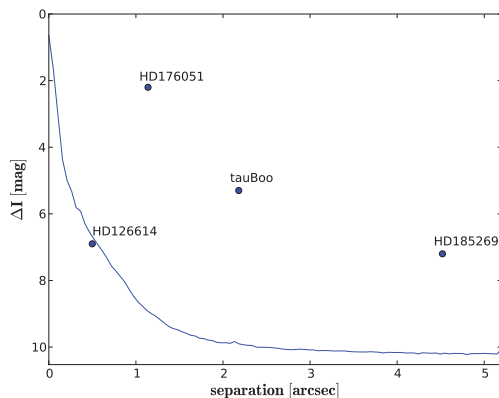


Figure 14. Average dynamic range in all observation epochs after PSF subtraction. All detected stellar companions have been added. The typical standard deviation is 0.2 mag.

known stellar multiple systems harbouring extrasolar planets, we refer to Röll et al. (2011b).

We will continue our current monitoring campaign in order to determine the multiplicity status of all exoplanet host stars, which then will yield the true multiplicity rate of planet-bearing stars. This will also eventually allow us to draw conclusions about the frequency of planets in multiple stellar systems, as well as their properties compared to planets which reside around single stars.

ACKNOWLEDGMENTS

CG and TE wish to acknowledge Deutsche Forschungsgemeinschaft (DFG) for grant NE 515/30-1. MS would like to thank DFG for support in project NE 515/36-1. Based on observations collected at the Centro Astronómico Hispano Alemán (CAHA) at Calar Alto, operated jointly by the Max-Planck Institut für Astronomie and the Instituto de Astrofísica de Andalucía (CSIC). We would especially like to express our thanks to the very helpful staff at the Calar Alto observation site. We used Simbad and VizieR as well as archival data from *HST*. *HST* data were obtained from the data archive at the Space Telescope Institute, which is operated by the association of Universities for Research in Astronomy, Inc., under the NASA contract NAS 5-26555. This publication makes use of data products from the Two Micron All Sky Survey, which is a joint project of the University of Massachusetts and the Infrared Processing and Analysis Center/California Institute of Technology, funded by the National Aeronautics and Space Administration and the National Science Foundation. This research has made use of the Washington Double Star Catalog maintained at the US Naval Observatory. We made use of the SciPy tools for scientific computation in PYTHON by Jones et al. (2001). CG would also like to

express special thanks to Tristan Röll and Christian Adam for their invaluable help and comments regarding the PYTHON programming language as well as Tobias Schmidt and Hiroshi Kobayashi for fruitful discussion. Finally, we would like to thank Donna Keeley for the language editing of our manuscript.

REFERENCES

- Baraffe I., Chabrier G., Allard F., Hauschildt P. H., 1998, *A&A*, 337, 403
 Bertin E., Arnouts S., 1996, *A&A*, 117, 393
 Chauvin G., Beust H., Lagrange A.-M., Eggenberger A., 2011, *A&A*, 528, 8
 Cutri R. M. et al., 2003, 2MASS All-Sky Catalog of Point Sources (Cutri+ 2003), VizieR Online Data Catalog
 Daemgen S., Hormuth F., Brandner W., Bergfors C., Janson M., Hippler S., Henning T., 2009, *A&A*, 498, 567
 Duchêne G., DelgadoDonate E., Haisch K. E., Jr, Loinard L., Rodríguez L. F., 2007, in Reipurth B., Jewitt D., Keil K., eds, *Protostars and Planets V*. Univ. Arizona Press, Tucson, p. 379
 Ford E. B., Kozinsky B., Rasio F. A., 2000, *ApJ*, 535, 385
 Fukugita M., Ichikawa T., Gunn J. E., Doi M., Shimasaku K., Schneider D. P., 1996, *AJ*, 111, 1748
 Hormuth F., 2007, Diploma thesis, Univ. Heidelberg
 Hormuth F., Hippler S., Brandner W., Wagner K., Henning T., 2008, Proc. SPIE, 7014, 138
 Howard A. W. et al., 2010, *ApJ*, 721, 1467
 Johnson J. A., Marcy G. W., Fischer D. A., Henry G. W., Wright J. T., Isaacson H., McCarthy C., 2006, *ApJ*, 652, 1724
 Jones E. et al., 2001, SciPy: Open Source Scientific Tools for python, <http://www.scipy.org/>
 Lada C. J., 2006, *ApJ*, 640, 63
 Law N. M., Mackay C. D., Baldwin J. E., 2006, *A&A*, 446, 739
 Mason B. D., Hartkopf W. I., Gies D. R., Henry T. J., Helsel J. W., 2009, *AJ*, 137, 3358
 Mathieu R. D., Ghez A. M., Jensen E. L. N., Simon M., 2000, in Mannings V., Boss A. P., Russell S. S., eds, *Protostars and Planets IV*. Univ. Arizona Press, Tucson, p. 703
 Mugrauer M., Neuhäuser R., 2009, *A&A*, 494, 373
 Mugrauer M., Seifahrt A., Neuhäuser R., 2007, *MNRAS*, 378, 1328
 Mutterspaugh M. W. et al., 2010, *AJ*, 140, 1657
 Patience J. et al., 2002, *ApJ*, 581, 654
 Roddier F., Gilli J. M., Lund G., 1982, *J. Opt.*, 13, 263
 Röll T., Seifahrt A., Neuhäuser R., Köhler R., 2011a, in Prsa A., Zejda M., eds, *ASP Conf. Ser. Vol. 435, Binaries: Key to Comprehension of the Universe*. Astron. Soc. Pac., San Francisco, p. 419
 Röll T., Seifahrt A., Neuhäuser R., Mugrauer R., 2011b, *A&A*, submitted
 Sánchez S. F., Aceituno J., Thiele U., Pérez-Ramírez D., Alves J., 2007, *PASP*, 119, 1186
 Schneider J., Dedieu C., Le Sidaner P., Savalle R., Zolotukhin I., 2011, *A&A*, 532, 79
 Söderhjelm S., 1999, *A&A*, 341, 121
 Takeda G., Rasio F. A., 2005, *ApJ*, 627, 1001
 van Leeuwen F., 2007, *A&A*, 474, 653

This paper has been typeset from a TeX/LaTeX file prepared by the author.